Lab on a Chip

RSC Publishing

PAPER

View Article Online
View Journal | View Issue

Label-free biodetection using a smartphone†

Cite this: *Lab Chip*, 2013, **13**, 2124

Dustin Gallegos,‡[a] Kenneth D. Long,‡[b] Hojeong Yu,‡[a] Peter P. Clark,[c] Yixiao Lin,[a] Sherine George,[b] Pabitra Nath[a] and Brian T. Cunningham*[ab]

Received 29th August 2012,
Accepted 3rd April 2013

DOI: 10.1039/c3lc40991k

www.rsc.org/loc

Utilizing its integrated camera as a spectrometer, we demonstrate the use of a smartphone as the detection instrument for a label-free photonic crystal biosensor. A custom-designed cradle holds the smartphone in fixed alignment with optical components, allowing for accurate and repeatable measurements of shifts in the resonant wavelength of the sensor. Externally provided broadband light incident upon an entrance pinhole is subsequently collimated and linearly polarized before passing through the biosensor, which resonantly reflects only a narrow band of wavelengths. A diffraction grating spreads the remaining wavelengths over the camera's pixels to display a high resolution transmission spectrum. The photonic crystal biosensor is fabricated on a plastic substrate and attached to a standard glass microscope slide that can easily be removed and replaced within the optical path. A custom software app was developed to convert the camera images into the photonic crystal transmission spectrum in the visible wavelength range, including curve-fitting analysis that computes the photonic crystal resonant wavelength with 0.009 nm accuracy. We demonstrate the functionality of the system through detection of an immobilized protein monolayer, and selective detection of concentration-dependent antibody binding to a functionalized photonic crystal. We envision the capability for an inexpensive, handheld biosensor instrument with web connectivity to enable point-of-care sensing in environments that have not been practical previously.

Introduction

Since their introduction in 1997 ''smart'' mobile phones with internet connectivity, high resolution cameras, touch-screen displays, and powerful CPUs have gained rapid market acceptance.[1] It is estimated that, of the >5.6 billion mobile phones that are currently in use,[2] 20% of them can be classified as smartphones, with an expected rise to ~40% by 2015.[3] The rapid acceptance of smartphones is driven by a combination of falling prices and increasingly sophisticated features. In addition, there is a growing ecosystem of applications that take advantage of the phone's sensors, display, and connection to powerful computing and data storage capabilities that are available in the ''cloud.'' The built-in capabilities of smartphones can be further extended through the addition of accessories that enable the phone to sense different types of information. For example, it is already possible to find commercial lens systems that enable the phone to be used as a rudimentary microscope with 350× magnification – sufficient for capturing images of cells, bacteria, and biological tissue.[4,5] It has also been recently demonstrated that, with addition of a light collimation system and a diffraction grating in front of the camera, a smartphone may also function as a spectrometer with a wavelength resolution of 5 nm.[5] The ability of the smartphone camera to take images of the colored label components of a biological assay have been applied to lateral flow immunoassays[6] quantum-dot labeling of bacteria[7] and fluorescence microscopy.[4] Furthermore, smartphone cameras have recently been exploited for microfluidic and optofluidic applications[8,9] and as a lens-free microscopy tool.[10]

Incorporation of biosensing into smartphone platforms is a potentially powerful development, as biological assay capabilities that have previously only been available through expensive laboratory-based instruments may be utilized by anyone. Such developments may help to facilitate the goal of ''personalized medicine'' in which home-based tests may be used to diagnose a medical condition, but with a system that automatically communicates results to a cloud-based monitoring system that alerts the physician when warranted. Low-cost portable biosensor systems integrated with smartphones may also enable diagnostic technology that can be translated to resource-poor regions of the world for pathogen detection, disease diagnosis, and monitoring of nutritional status. Such a

[a]*Department of Electrical and Computer Engineering, Micro and Nanotechnology Laboratory, University of Illinois at Urbana-Champaign, 208 North Wright Street, Urbana, IL, 61801, USA. E-mail: bcunning@illinois.edu*
[b]*Department of Bioengineering, Micro and Nanotechnology Laboratory, University of Illinois at Urbana-Champaign, 208 North Wright Street, Urbana, IL, 61801, USA*
[c]*Lensvector Inc, 6 Clock Tower Place, Maynard, MA 01754, USA*

† Electronic supplementary information (ESI) available. See DOI: 10.1039/c3lc40991k

‡ Co-authors who contributed equally to this work, listed alphabetically

system, deployed widely, would be capable of rapidly monitoring for the presence of environmental contaminants over large areas, or tracking the development of a medical condition throughout a large population. While ELISA-based biological assays can be applied to the detection of many biological analytes, their widespread adoption into scenarios outside the laboratory is hindered by the complexity of the assay protocol, which involves the use of an enzyme-tagged secondary antibody and a color-generating substrate.[11–14] Detection of an analyte through one of its intrinsic physical properties (dielectric permittivity, mass, conductivity, or Raman scattering spectrum – for example), called ''label-free'' detection,[15–17] is preferable for assay simplicity in terms of the number of reagents required, washing steps needed, and assay time.

Of all the label-free detection approaches that have been demonstrated, those based upon optical phenomena have been most commercially accepted due to a combination of sensitivity, sensor cost, detection system robustness, and high throughput. Adsorption of biomolecules, viral particles, bacteria, or cells on the surface of an optical biosensor transducer results in a shift in the conditions of optimal optical coupling, which can be measured by illuminating the transducer surface, and subsequently measuring a property of the reflected or transmitted light. Such a detection approach is extremely robust, and has become economically advantageous due to the advent of low cost light emitting diodes, semiconductor lasers, and miniature spectrometers. For example, surface plasmon resonance (SPR) based biosensors[18–22] and photonic crystal (PC) optical biosensors[23–27] are capable of detecting broad classes of biological analytes through their intrinsic dielectric permittivity. Each approach has been implemented in the form of large laboratory instruments, and miniaturized (shoebox-sized) systems. No prior label-free optical biosensor instrument has been fully integrated with a smartphone, using the camera in the phone itself as the detection instrument.

Here, we demonstrate the use of a smartphone to detect shifts in the resonant wavelength of a photonic crystal (PC) label-free biosensor. PC biosensors are especially amenable to readout by a smartphone, as they function as narrow bandwidth reflection filters that are measured by illuminating them at normal incidence with collimated white light. The PC used in this work was designed to produce a high efficiency resonant reflection at a wavelength in the visible spectrum (λ = 565 nm) in a dry environment. Adsorption of biomolecules on the PC surface results in a shift of the resonant wavelength to larger values. To enable the phone camera to measure the PC resonance, we have designed and constructed a custom cradle that provides an aligned optical interface between the camera, the PC, and a series of optical components. While the phone and the optical components are held fixed, the sensor itself may be inserted and removed from a narrow slot within the cradle. In order to automate and make the process of taking biosensor measurements truly portable, we have developed a smartphone software application that converts camera images into spectra, fits the spectra to a mathematical function to determine the PC resonant wavelength, and displays the results (Screenshots from the App displayed in Supplemental Information). Importantly, the system incorporates the ability to compare wavelength shifts from adjacent ''active'' and ''reference'' regions of the PC, as a means for incorporating an accurate experimental control. To demonstrate operation of the sensor and detection system, we detect adsorption of a protein monolayer on the PC[28] and perform dose/response characterization of porcine immunoglobulin G capture by an immobilized layer of Protein A.[29]

Methods

PC Biosensor operating principle, structure, and fabrication

The PC is comprised of a 1-dimensional grating surface structure that is produced on a flexible plastic substrate from a UV-curable polymer by a nanoreplica molding process as described in previous publications.[30,31] In this case, the PC grating period is 360 nm and the grating depth is d = 60 nm. The polymer grating is subsequently over-coated with sputtered thin films of SiO_2 (t = 200 nm) and TiO_2 (t = 60 nm, refractive index = 2.35). After fabrication, the flexible plastic substrates were attached to standard 1 × 3 in^2 glass microscope slide using double-sided pressure-activated adhesive film. The grating dimensions and thin film thicknesses are designed to enable the structure to behave as a high efficiency narrowband reflectance filter with a center wavelength of λ = 565 nm and a resonance bandwidth (full width at half-maximum: FWHM) of $\lambda \sim 5$ nm when the surface of the PC is dry. When illuminated by collimated light at normal incidence, all wavelengths easily transmit through the PC, except for the resonantly reflected wavelength, which is reflected with >95% efficiency, as shown schematically in Fig. 1. Adsorption of biomolecular material on the PC surface results in an increase of the effective refractive index of the resonant mode, resulting in a positive shift in the wavelength of resonant reflection, whose magnitude is proportional to the optical density of the deposited material. Therefore, our system is arranged to measure shifts in the Peak Wavelength Value (PWV) of minimum transmission efficiency (or equivalently a maximum in reflection efficiency) that occur as a result of a biological assay.[32]

Smartphone cradle optical system

An iPhone 4 (Apple, Inc., Cupertino, CA, USA) was used as the smartphone, requiring fabrication of a cradle that securely holds the phone's back camera in alignment with the PC and the detection optics. The cradle allows operation of the smartphone through its touchscreen interface while the user inserts/removes the sensor from the back of the unit. Our prototype cradle was made of anodized machined aluminum, although an equivalent fixture could also be constructed from injection molded plastic. A schematic diagram of the detection system is shown in Fig. 2. Unpolarized light from an external broadband source enters the system through a pinhole (diameter = 100 μm) and a collimating lens (focal length =

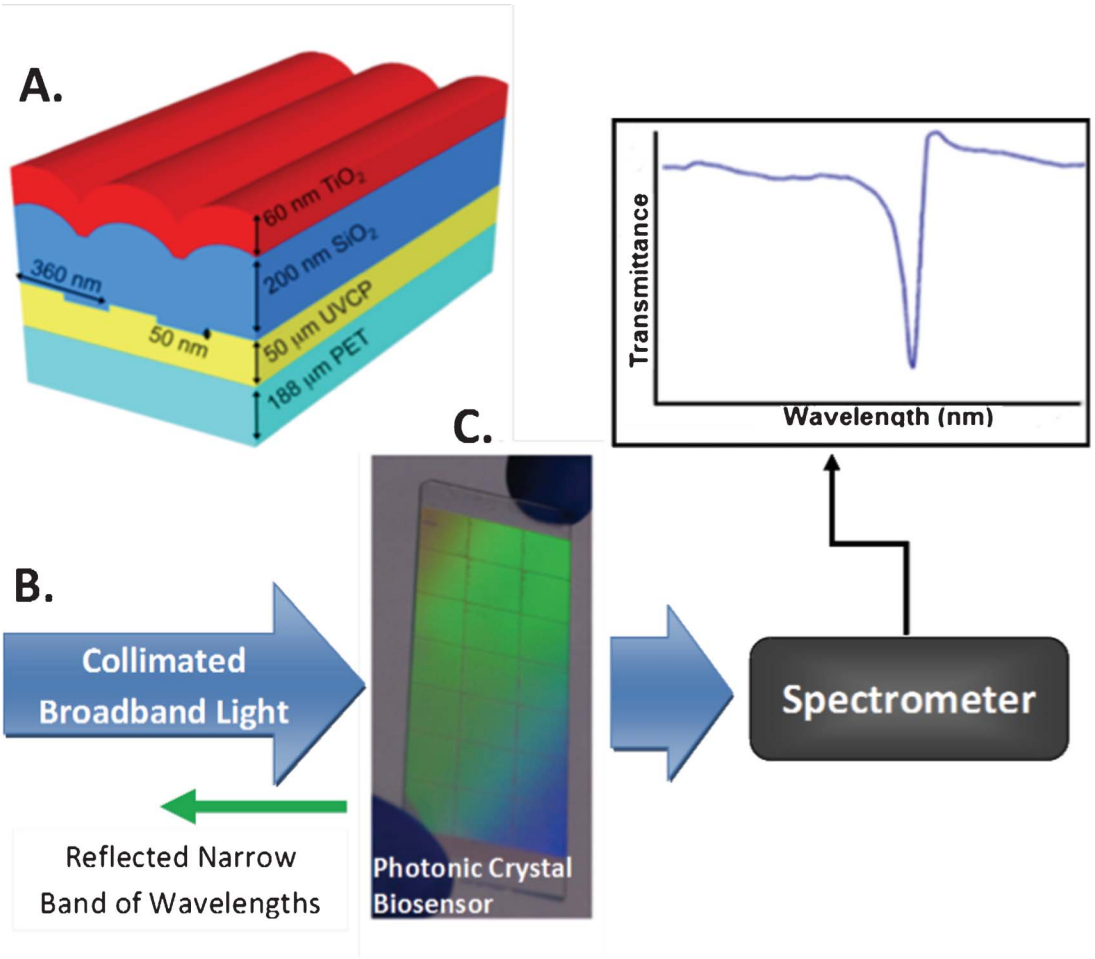

Fig. 1 A. Cross section schematic of the PC structure. B. Operating principle of the PC biosensor. When the structure is illuminated with a wide range of wavelengths, only a narrow band of wavelengths is reflected, while all other wavelengths transmit through without attenuation. C. Photograph of a photonic crystal attached to a 1 × 3 in^2 glass microscope slide.

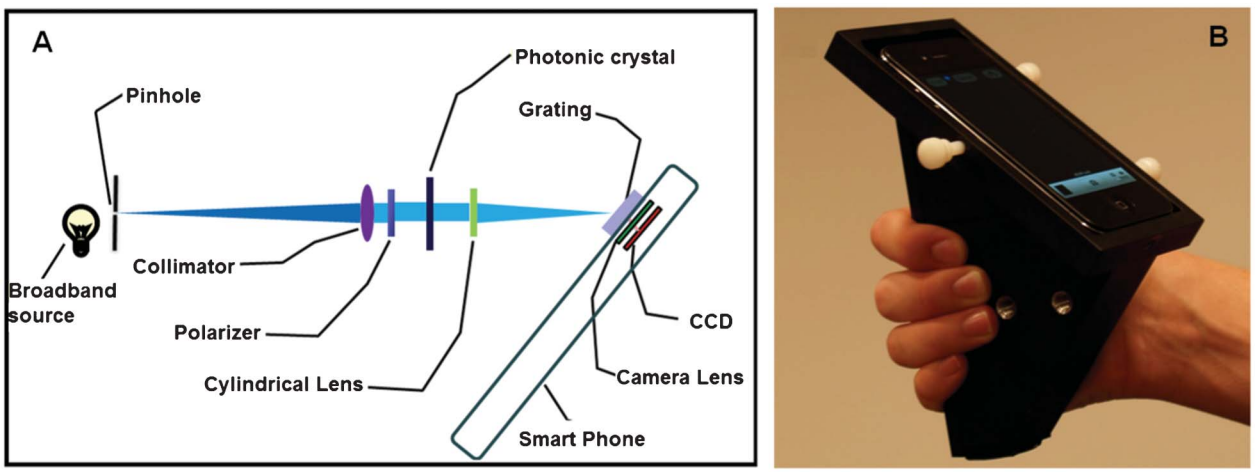

Fig. 2 A. Schematic of the optical components within the smartphone cradle. Broadband light from an external source (such as an incandescent lamp or LED) is collimated by the combination of an entrance pinhole and a collimating lens. After passing through a linear polarizing filter, light passes through the PC, which resonantly reflects one narrow band of wavelengths. The cylindrical lens increases the amount of light that is collected by the camera. B. Photo of the cradle with a PC biosensor slide inserted into the detection slot.

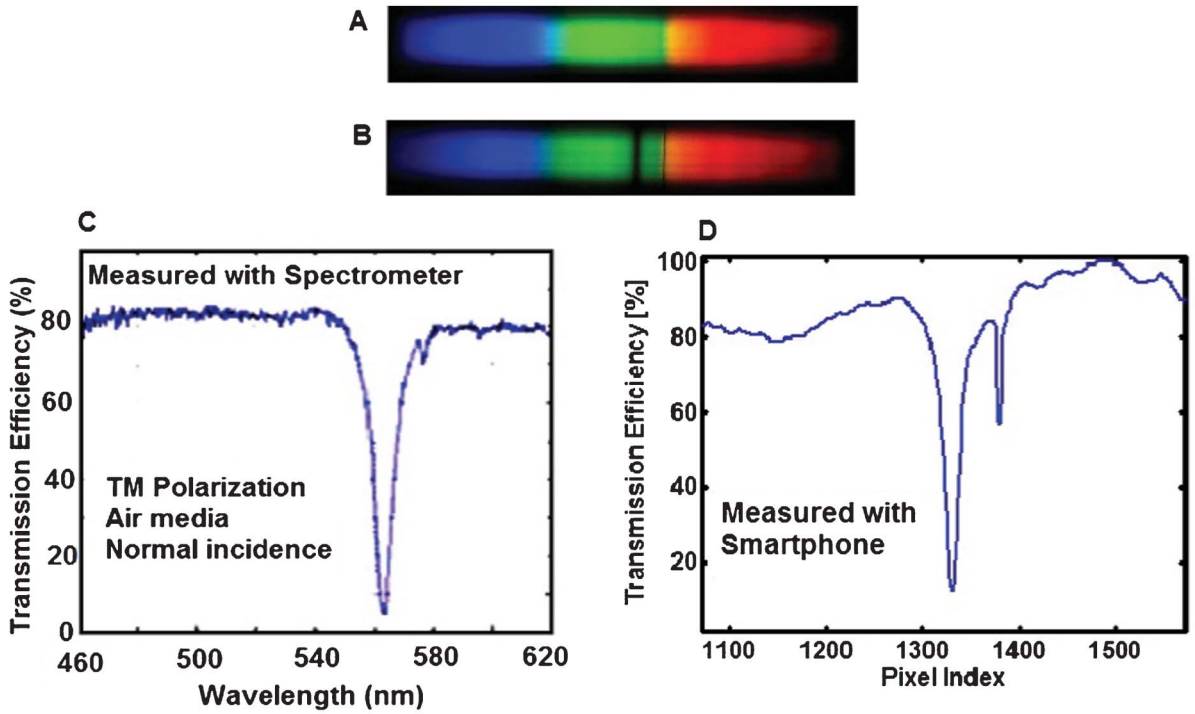

Fig. 3 A. A ''rainbow'' band corresponding to a range of wavelengths in the visible spectrum lies across the image. The absence of a narrow range of wavelengths produces the dark line in the middle of the spectrum band. B. The resulting Transverse Magnetic (TM) transmission profile of the PC as seen by the smartphone's CCD in terms of pixels. The ''dip'' corresponds to the missing wavelengths reflected by the PC. C. The analogous spectrum reading for the same PC when measured *via* spectrometer. D. The analogous spectrum reading for the same PC when measured *via* smartphone detection system.

75 mm) before passing through a linear polarizing filter that is oriented to pass only light with its electric field vector perpendicular to the PC grating lines. The collimated and polarized light passes through the PC at normal incidence, so all the incident light may pass forward, with the exception of the PC resonant wavelength band. A slot for the PC is incorporated into the optical chain, so that the sensor may be easily inserted and removed. Small markings were made on the PC slide, so a specific location could be re-measured during distinct steps in the assay process. After passing through the PC, the light is focused to a line by a cylindrical lens (focal length = 50 mm), onto the entrance pupil of the smartphone's camera. A diffraction grating (1200 lines mm^{-1}) placed between the cylindrical lens and the camera disperses the wavelength components of the light across the camera's CMOS image sensor. The diffraction angle of the grating's first order results in the need to orient the optical path through the PC at an angle of $\sim 47^{\circ}$ with respect to the camera face. The camera provides sensitivity to wavelengths in the visible spectrum, thus the dispersed broadband light results in a digital image that appears as a ''rainbow'' band corresponding to the $400 < \lambda < 650$ nm when the entrance pinhole is illuminated with a tungsten incandescent lamp, as shown in Fig. 3a. Although the iPhone4 camera image sensor has a total of 5 megapixels (2592 × 1936), the spectrum band covers approximately 750 pixels in the dispersive direction and it is roughly 100 pixels wide. Assuming a focal length of the iPhone4 lens of 3.85 mm, the wavelength separation between adjacent pixels in the spectral direction will be 0.333 nm $pixel^{-1}$. As shown in Fig. 3b, when the PC is inserted into the optical path, a narrow band of wavelengths is removed from the transmitted spectrum, resulting in a dark band in the image that is easily observed. A resonant transmission ''dip'' from the PC with a bandwidth of 5 nm is expected to be measured by ~15 pixels. The retail cost of the optical components in the system is ~$210 US Dollars (See Supplementary Information for a detailed list of components and additional images†).

Smartphone biosensor software application

An iPhone software application (App) was developed to facilitate the gathering of spectra, measuring the PWV of the PC, and determining PWV shifts. The App first prompts the user to enter information about a measurement, such as the sample name. Additional global settings can be adjusted by the user to control filtering parameters, intensity threshold, and the span of pixels from the center of the resonant band to be considered during curve fitting. To achieve the highest spectral resolution, the camera must be focused at infinity. This is done by pointing the camera to a distant object in a well-lit environment before placing the iPhone into the cradle. The App locks the focal distance of the camera at infinity for all subsequent measurements.

Tapping the ''Capture'' button within the App triggers the following events: A rapid sequence of spectra images (five were used for the work reported here) are captured consecutively to

minimize the effects of small intensity fluctuations that arise from the light source and camera's sensor. To obtain an intensity spectrum profile from each spectra image, the App first crops the image to thirty pixels gathered from the center of the 100-pixel wide spectral band, discarding dark pixels above and below the band. The 30-pixel values taken from the band are averaged to yield a single intensity value for every wavelength of the spectrum for each of the five consecutive images, resulting in a one dimensional array (1×2592 pixels) per image captured. The five spectra gathered from independent consecutive images are finally averaged to yield a single spectrum. This process takes approximately two seconds. As discussed in Results, the system has been calibrated to correlate pixel values with specific wavelength values.

The App stores the spectrum of the light source before a PC is inserted into the cradle, which is used to normalize the spectrum after the PC is inserted into the optical path to yield the PC transmission efficiency plot shown in Fig. 3c. The transmission spectrum for the PC measured with the smartphone system closely matches the transmission spectrum obtained by illuminating the PC with the collimated output of an optical fiber and measuring the transmission efficiency with a conventional spectrometer (Fig. 3d).

Finally, the App processes the PC transmission spectrum to determine the PWV for the measurement. The App identifies the pixel in the spectrum with the lowest intensity value, and then uses the 20-pixel values surrounding this point to fit the ''dip'' to a third-order polynomial function. The PWV is mathematically determined as the minima of the polynomial as discussed in.[33] In this way, PWV shifts $\sim 10\times$ smaller than the wavelength increments of the camera can be measured. Gathering sequential PWV measurements of a sensor without removal/insertion in the cradle results in a standard deviation of $\sigma = 0.003$ nm. Therefore, the smallest PWV shift that can be measured with the system is $3\sigma = 0.009$ nm. The App enables wireless transmission of all spectra and PWV measurements.

Measurement protocol

Using the instrument and software, an assay is performed in the following fashion: the PC is initially prepared by immobilizing a capture molecule (such as an antibody, aptamer, or single-strand DNA sequence) that selectively recognizes the analyte in a test sample. The sensor surface is further prepared with a ''blocking'' step that prevents nonspecific adsorption of other molecules. The PWV of the sensor is measured prior to the test sample addition to establish a baseline reading. Exposure of the sensor to the test sample results in adsorption of the analyte upon the PC, followed by rinsing/drying the sensor. A second PWV measurement is taken of the sensor, and the PWV shift is determined by subtraction of the baseline PWV. The basic approach outlined in this protocol can be augmented by the incorporation of positive and negative experimental controls, including the use of a ''reference'' sensor that is prepared with an unmatched capture molecule, but still exposed to the test sample. Although all measurements reported here were taken with the PC surface in a dry state, the system can be further augmented *via* incorporation of a static liquid chamber or flow cell on the PC, so the PWV shifts can be monitored kinetically.

Results

Wavelength calibration

Pixel values in the smartphone image were translated to calibrate the wavelength values through the use of two laser pointers and a calibrated spectrometer (HR2000 fiber optic spectrometer, Ocean Optics, Dunedin, FL, USA). As shown in Fig. 4a, a green and a red laser pointer were used to illuminate the tip of an optical fiber with its distal end connected to the spectrometer, resulting in the dashed curves with peak intensity values at wavelengths of $\lambda = 533.91$ nm and $\lambda = 656.26$ nm. The same laser pointers were then used to illuminate the pinhole of our smartphone detection instrument, resulting in the solid curves. Assuming linearity between the image pixel value and wavelength with two known values of wavelength, we derive a transfer function that translates every pixel value into a wavelength value for all subsequent measurements. The distance (366 pixels) between laser index values is translated into a wavelength index through the conversion factor 0.334 nm pixel^{-1}, closely matching our prediction.

Also shown in Fig. 4a is a comparison of the spectra from the tungsten lamp illumination source taken by the spectrometer and the smartphone. We observe a drop off in intensity as the wavelength increases beyond $\lambda = 580$ nm and a complete loss of sensitivity to wavelengths greater than $\lambda = 680$ nm, attributed to an internal low-pass filter. The PC used in this work is designed for operation in the $550 < \lambda < 580$ nm range in order to take advantage of the wavelengths available with good sensitivity from the camera.

Measurements of transmission spectra from a PC

Using the pixel-to-wavelength mapping outlined above, we sought to characterize the repeatability of independent PWV measurements, when the PC is removed/reinserted from the cradle without intentionally introducing any other variable. Fig. 4b shows 13 overlaid spectra from independent measurements when the sensor is removed and replaced within the cradle, as would be the case when a biological assay is performed. The spectra are observed to have a mean PWV = 565.77 nm, and a standard deviation of $\sigma = 0.003$ nm, demonstrating that measurements are highly reproducible and that wavelength shifts greater than $3\sigma = 0.009$ nm are statistically meaningful in the context of biological assays.

Measurements of PWV shift

Having demonstrated the ability of this instrument to make repeatable assessments we next sought to measure shifts in the PC wavelength that are intentionally introduced by addition of material to the PC surface.

First, we prepared a PC upon which we deposited a thin film of SiO_2 by RF sputtering (PVD 250, Kurt Lesker, Jefferson Hills, PA, USA) on one half of a PC sensor, while leaving the other half uncoated. Using a standard spectrometer, we first measured the shift in the PWV for the SiO_2 coated PC and compared it to the bare PC region measuring $\Delta PWV = 5.11$ nm. We then measured the transmission spectrum for the same regions of the PC using the smartphone detection system. Fig. 5a shows the spectra for the bare PC and the SiO_2-coated

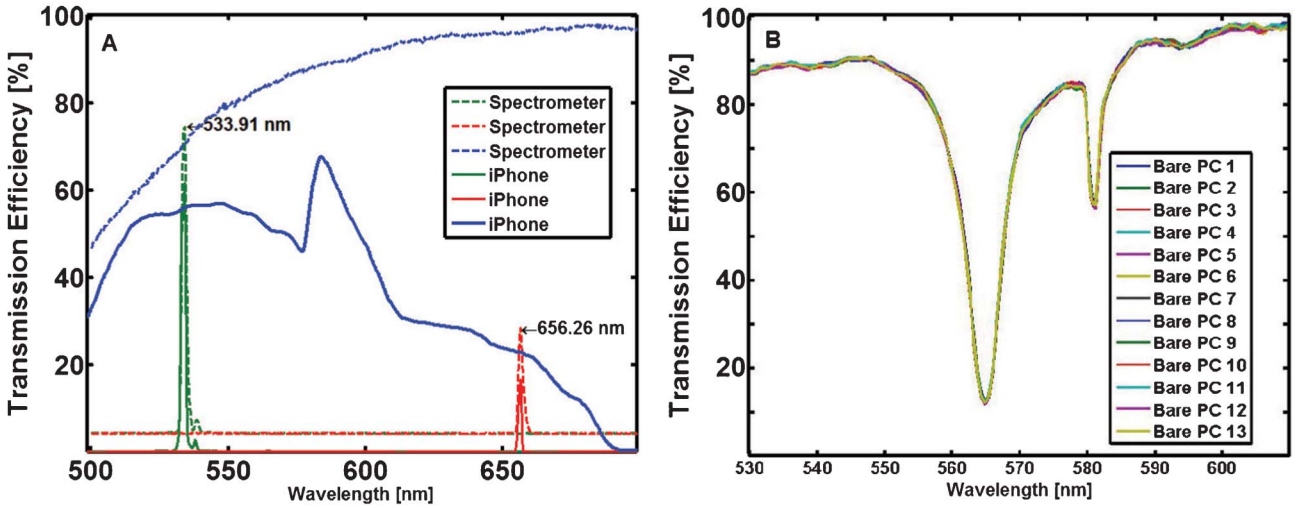

Fig. 4 A. Overlaid spectra from red and green laser pointers measured with a calibrated spectrometer (dashed curves) and the smartphone (solid curves) used to obtain a translation factor from pixels to wavelength values. B. The transmission spectra of 13 independent PC spectra taken by removing and re-inserting the PC into the cradle, demonstrating excellent measurement reproducibility.

PC, demonstrating a shift of ΔPWV = 5.08 nm. Using a finite-difference time domain (FDTD solutions, Lumerical, Vancouver, BC, Canada) computer model of the fabricated PC structure, we calculated the PWV shift from the addition of an SiO_2 film with the known refractive index of that material produced by our sputter system (n = 1.45). The FDTD model predicts that a 13 nm thick layer of SiO_2 deposited on the PC structure will result in a PWV shift of 5 nm.

Next, we sought to measure the PWV shift induced by adsorption of a protein monolayer. The protein polymer poly-phe-lysine (PPL, Sigma Aldrich) is well-known to adhere to dielectric surfaces, such as the PC, forming a 15 nm thick layer that self-limits to a single monolayer.[34,35] We first gathered a baseline spectrum from a specific location of a PC biosensor in its "bare" state, and then placed a temporary rubber gasket over that location to create a 3 mm liquid-containment well. The well was filled with 100 μL of PPL diluted in deionized water at a concentration of ~1 mg ml^{-1}, and allowed to incubate on the PC surface for 120 min at room temperature. After incubation, the PPL solution was removed and the well was flushed with deionized water. The gasket was removed, and the PC was further rinsed and dried with N_2 before returning the PC to the detection system for a second spectral measurement. Results of this experiment are shown in Fig. 5b in which ΔPWV = 1.66 nm is measured.

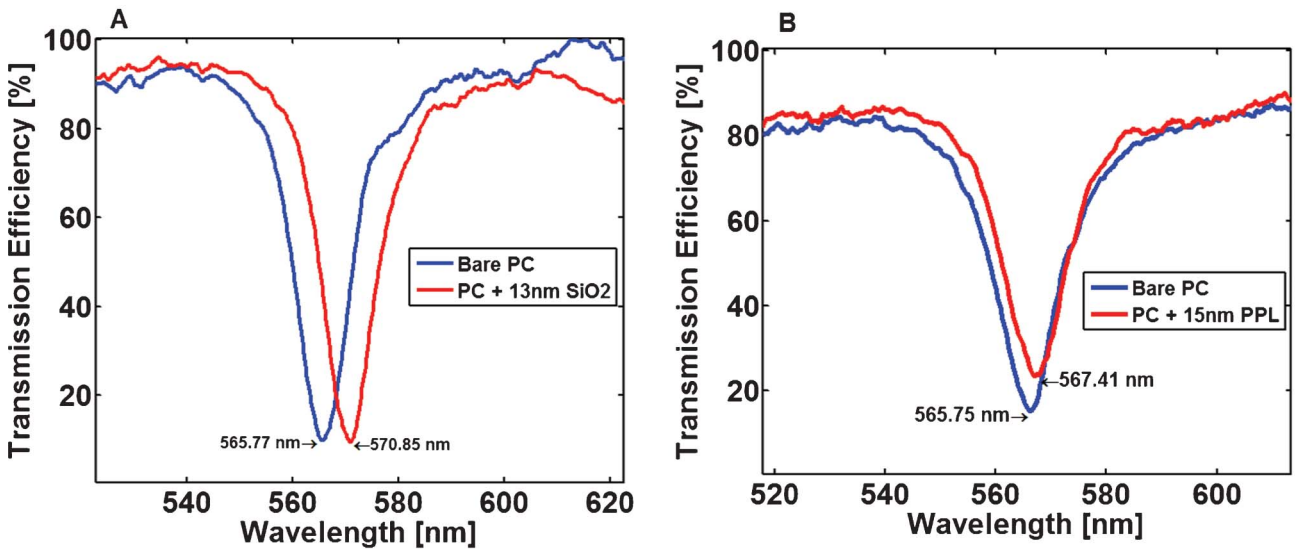

Fig. 5 A. Normalized transmission characteristics for a bare PC and an adjacent region of the same PC coated with a SiO_2 thin film, resulting in a positive shift of the measured PWV. B. Transmission spectra of a PC before and after deposition of a monolayer of PPL protein.

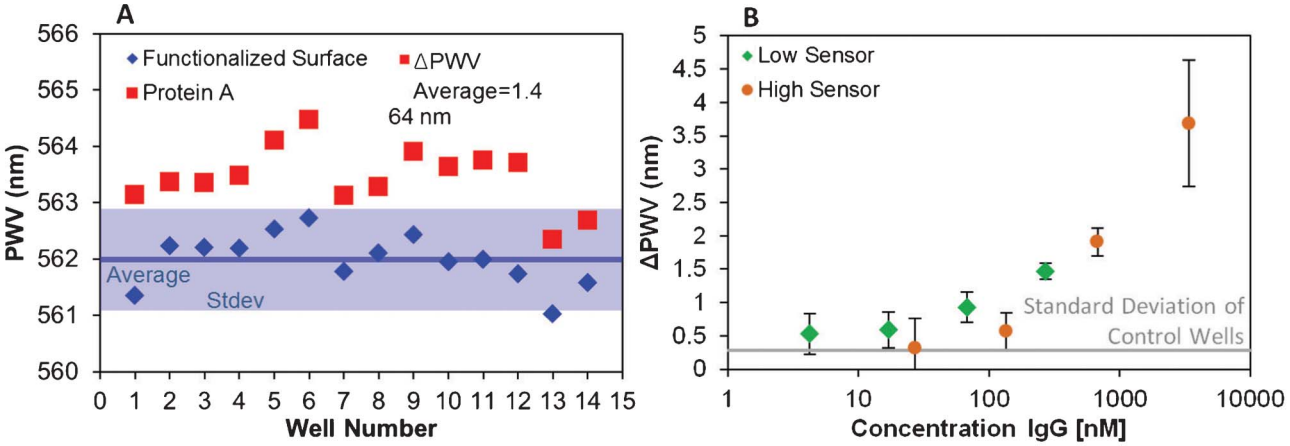

Fig. 6 Concentration dependent PWV shift of porcine IgG antibody. A. Variation in slide functionalization *versus* Protein A deposition. B. Protein A was immobilized on two PC sensors to detect concentrations of porcine IgG antibody present in quantities between 1 nM and 5000 nM. $N = 3$ for assay wells; $N = 2$ for control wells.

Biodetection demonstration of the smartphone instrument

Finally, we demonstrate the ability of the sensor and detection instrument to perform a biodetection assay in which a layer of immobilized capture molecule is able to selectively capture a specific biomolecule of interest. As a representative example, we demonstrate the capture of porcine immunoglobulin G (IgG) using an immobilized layer of Protein A.

The PC sensor was functionalized with an aldehyde-based surface chemistry to facilitate the attachment of Protein A. To begin the surface preparation procedure, the PC slide was thoroughly cleaned using an acetone/IPA/DI-H_2O wash, and then functionalized with a 10% solution of polyvinylamine in water at 40 °C for two hours. It was then washed 3× in ultrapure water, and incubated in a 25% solution of glutaraldehyde in water (Sigma Aldrich) for 4 h at room temperature. After a subsequent triplicate wash in ultrapure water and drying of the sensor surface, the PWVs from 14 distinct locations on the functionalized PC surface were recorded by the smartphone detection instrument to establish the baseline PWV upon which subsequent wavelength shifts caused by the attachment of capture and target molecules would be compared.

Next, a custom-made polydimethylsiloxane (PDMS) gasket was adhered to the PC sensor surface to form 14 separate assay wells (diameter = 6 mm) over the 14 measurement locations. Each well was incubated with 60 μL of 0.5 mg mL^{-1} Protein A in .01 M phosphate buffered solution (PBS; pH = 7.4) for 20 min. After Protein A immobilization, the wells were washed with PBS, the gasket was removed, and the PC sensor was dried. A second PWV reading was gathered from each location, in order to establish the PWV shift due solely to the attachment of the Protein A layer. Fig. 6a shows the initial PWV associated with each of the 14 wells on a single PC sensor, and the PWV shift induced at each location by Protein A deposition, demonstrating the initial variability induced by the PC functionalization (average PWV = 561.99 nm, stdev = 0.464 nm), and the PWV shift induced by the Protein A deposition process (average ΔPWV = 1.46 nm, stdev = 0.288 nm). These results demonstrate that the protein attachment process used here introduces a greater degree of variability than the sensors themselves, or the variability of sensor measurements from the smartphone instrument.

Prior to the exposure of the PC sensor to the IgG analyte, the gasket was replaced, and the PC was rehydrated with 60 μL PBS in each well for 10 min. After aspiration, 60 μL of porcine IgG solutions were added to each well at concentrations ranging from 4.25 nM to 3.4 μM (Fig. 6b) and incubated for 10 min. After a rinse with 0.01 M PBS to remove unbound antibody, the PC sensor was dried and measured using the smartphone to calculate the ΔPWV induced by IgG attachment. Concentration-dependent PWV shifts were observed, with each IgG concentration being measured in triplicate. Intra-sensor variability is low (average stdev for triplicate measurements was 0.335 nm). The lowest IgG concentration tested (4.25 nM) was observable above the negative control (0 nM IgG), indicating the ability to clearly measure wavelength shifts of 0.16 nm above sensor-specific background noise on that sensor (data not shown) that is limited by assay-related variability, rather than by the wavelength shift resolution of the detection instrument. Despite its compact size and simplicity, the detection instrument is capable of detecting the presence of analytes in the nM concentration range with a "direct" assay. The limits of detection of the system can be reduced further through the use of a variety of tags, such as secondary antibodies[36] or nanoparticles[37,38] that can amplify the wavelength shift by factors of 5–1000×.

Discussion

In this work, we present the first use of a smartphone as a detection instrument for a label-free optical biosensor. Using a cradle that incorporates several inexpensive optical components and hold them in alignment with the smartphone camera, we demonstrate that the camera can serve as a highly accurate spectrometer for measuring the transmission spectrum from a photonic crystal biosensor. The computational capability of the smartphone was used to guide the user

through the assay process *via* touchscreen commands, to perform image processing that converted a sequence of photos into a spectrum, and to convert the spectrum into a value that represents the resonant wavelength of the PC. Although the system is compact and inexpensive, it is highly sensitive. We demonstrated easily detectable resonant wavelength shifts induced by the deposition of a thin dielectric film, a protein monolayer, and a fractional monolayer of target analyte selectively bound by a capture layer. We also demonstrated a simple capability for multiplexing several biosensor measurements in the system by preparing a single PC biosensor surface that can mechanically be inserted into the fixture, where several independent locations can be measured.

For the practical utility of the apparatus, it is important for future versions of the smartphone biosensor to have the ability to use wet samples by allowing for the use of thicker cartridges comprised of 3D wells, as opposed to the current limitation of working with planar slides. The decision to take measurements of the PC surface in a dry state was dictated by the desire to measure sensors in as simple of a manner as possible, without the possibility for bulk refractive index effects, or the incorporation of fluid flow (with associated pumps and valves) into the instrument. Detection in a dry state also allows assay steps to be performed separately from the detection step in both time and physical location, which may be desirable for real-world detection scenarios we are considering. Incorporation of a microfluidic channel into the sensor through the fabrication of a more sophisticated cartridge would enable liquid-based detection and the potential for measuring the kinetics of analyte binding, and is certainly possible using the described sensing approach.

The experiments used to characterize the smartphone detection instrument presented in this paper serve to demonstrate the feasibility of measuring PWV shifts from a PC biosensor, rather than focusing on the application of the system to complex test samples that contain many potentially interfering compounds. In order to address this issue for such applications, it will be necessary to incorporate ''reference'' sensors that can serve as negative controls to the effects of nonspecific binding. Such methods, commonly reported in the biosensor literature, should include multiple types of negative controls. First, as shown in this work, a detection experiment should include a sensor that is prepared with the capture molecule, but that is exposed to buffer rather than to the test sample. Secondly, the experiment should also include a sensor that is prepared with a capture molecule that does not recognize the analyte (such as an antibody for a nonrelated antigen), and exposed to the test sample. The combination of these two experimental controls can determine the mass density of analyte molecules that are bound nonspecifically to the sensor surface from a complex media, while at the same time taking into account common mode error sources such as temperature variability or bulk refractive index variability.

Having demonstrated these basic capabilities, it is our future goal to apply this system to a greater range of assays. Smartphone-based detection systems are expected to find applications in situations where laboratory facilities are not available such as point-of-care analysis in the home, clinic, or remote locations. The data-sharing capabilities of smartphone-based sensors will enable distributed networks of sensors to be deployed across large physical areas, but with cloud-based systems that can collate and map data. Such systems can aid in the interpretation of sensor data, or make data readily available to clinicians who are not at the same location as the patient. We also expect that these capabilities can be extended to other varieties of biosensors and assays that can take advantage of spectroscopic data.

Notes and references

1 B. Reed, *A brief history of smart phone*, 2010, www.pcworld.-com/.
2 N. Wang, ITU October 11, 2012, Press Release, www.itu.int.
3 ''Market information and statistics'' 2012, www.itu.int.
4 D. N. Breslauer, R. N. Maamari, N. A. Switz, W. A. Lam and D. A. Fletcher, *PLoS One*, 2009, **4**, e6320.
5 Z. J. Smith, K. Q. Chu, A. R. Espenson, M. Rahimzadeh, A. Gryshuk, M. Molinaro, D. M. Dwyre, S. Lane, D. Matthews and S. Wachsmann-Hogiu, *PLoS One*, 2011, **6**, e17150.
6 O. Mudanyali, S. Dimitrov, U. Sikora, S. Padmanabhan, I. Navruz and A. Ozcan, *Lab Chip*, 2012, **12**, 2678–2686.
7 H. Y. Zhu, U. Sikora and A. Ozcan, *Analyst*, 2012, **137**, 2541–2544.
8 A. W. Martinez, S. T. Phillips, E. Carrilho, S. W. Thomas, H. Sindi and G. M. Whitesides, *Anal. Chem.*, 2008, **80**, 3699–3707.
9 H. Y. Zhu, S. Mavandadi, A. F. Coskun, O. Yaglidere and A. Ozcan, *Anal. Chem.*, 2011, **83**, 6641–6647.
10 D. Tseng, O. Mudanyali, C. Oztoprak, S. O. Isikman, I. Sencan, O. Yaglidere and A. Ozcan, *Lab Chip*, 2010, **10**, 1787–1792.
11 V. A. U. F. de Souza, A. F. Tateno, R. R. Oliveira, R. B. Domingues, E. S. Araujo, G. W. Kuster and C. S. Pannuti, *J. Clin. Virol.*, 2007, **39**, 230–233.
12 J. Dasso, J. Lee, H. Bach and R. G. Mage, *J. Immunol. Methods*, 2002, **263**, 23–33.
13 S. X. Leng, J. E. McElhaney, J. D. Walston, D. Xie, N. S. Fedarko and G. A. Kuchel, *J. Gerontol., Ser. A*, 2008, **63**, 879–884.
14 Y. Y. Wu, A. M. Hruszkewycz, R. M. Delgado, A. Yang, A. O. Vortmeyer, Y. W. Moon, R. J. Weil, Z. P. Zhuang and A. T. Remaley, *Clin. Chim. Acta*, 2000, **293**, 199–212.
15 B. T. Cunningham and L. G. Liang, *Expert Opin. Drug Discovery*, 2008, **3**, 891–901.
16 A. Barhoumi and N. J. Halas, *J. Am. Chem. Soc.*, 2010, **132**, 12792–12793.
17 S. Ray, G. Mehta and S. Srivastava, *Proteomics*, 2010, **10**, 731–748.
18 X. Guo, *J. Biophotonics*, 2012, **5**, 483–501.
19 J. Homola, H. Vaisocherova, J. Dostalek and M. Piliarik, *Methods*, 2005, **37**, 26–36.
20 A. Kausaite-Minkstimiene, A. Ramanaviciene and A. Ramanavicius, *Analyst*, 2009, **134**, 2051–2057.

21 S. Lofas, M. Malmqvist, I. Ronnberg, E. Stenberg, B. Liedberg and I. Lundstrom, *Sens. Actuators, B*, 1991, **5**, 79–84.
22 J. G. Quinn, S. O'Neill, A. Doyle, C. McAtamney, D. Diamond, B. D. MacCraith and R. O'Kennedy, *Anal. Biochem.*, 2000, **281**, 135–143.
23 L. L. Chan, S. L. Gosangari, K. L. Watkin and B. T. Cunningham, *Apoptosis*, 2007, **12**, 1061–1068.
24 C. J. Choi, I. D. Block, B. Bole, D. Dralle and B. T. Cunningham, *IEEE Sens. J.*, 2009, **9**, 1697–1704.
25 D. Threm, Y. Nazirizadeh and M. Gerken, *J. Biophotonics*, 2012, **5**, 1–16.
26 N. Skivesen, A. Tetu, M. Kristensen, J. Kjems, L. H. Frandsen and P. I. Borel, *Opt. Express*, 2007, **15**, 3169–3176.
27 W. Zhang, N. Ganesh, I. D. Block and B. T. Cunningham, *Sens. Actuators, B*, 2008, **131**, 279–284.
28 M. Lee and P. M. Fauchet, *Opt. Express*, 2007, **15**, 4530–4535.
29 H. Ogi, K. Motohisa, K. Hatanaka, T. Ohmori, M. Hirao and M. Nishiyama, *Biosens. Bioelect.*, 2007, **22**, 3238–3242.
30 C. J. Choi and B. T. Cunningham, *Lab Chip*, 2007, **7**, 550–556.
31 C. J. Choi and B. T. Cunningham, *Lab Chip*, 2006, **6**, 1373–1380.
32 L. L. Chan, P. Y. Li, D. Puff and B. T. Cunningham, *Sens. Actuators, B*, 2007, **120**, 392–398.
33 I. D. Block, P. C. Mathias, N. Ganesh, S. I. Jones, B. R. Dorvel, V. Chaudhery, L. O. Vodkin, R. Bashir and B. T. Cunningham, *Opt. Express*, 2009, **17**, 13222–13235.
34 B. Lin, J. Qiu, J. Gerstenmeier, P. Li, H. M. Pien, J. Pepper and B. T. Cunningham, *Biosens. Bioelectron.*, 2002, **17**, 827–834.
35 M. Lu, S. S. Choi, C. J. Wagner, J. G. Eden and B. T. Cunningham, *Appl. Phys. Lett.*, 2008, **92**, 261502.
36 S. D. Soelberg, R. C. Stevens, A. P. Limaye and C. E. Furlong, *Anal. Chem.*, 2009, **81**, 2357–2363.
37 L. He, M. D. Musick, S. R. Nicewarner, F. G. Salinas, S. J. Benkovic, M. J. Natan and C. D. Keating, *J. Am. Chem. Soc.*, 2000, **122**, 9071–9077.
38 L. A. Lyon, M. D. Musick and M. J. Natan, *Anal. Chem.*, 1998, **70**, 5177–5183.

